International Journal of Electrochemical Science 18 (2023) 100264

Contents lists available at ScienceDirect

International Journal of Electrochemical Science

journal homepage: www.journals.elsevier.com/ijoes

Investigation of corrosion behavior of galvanized steel as submarine cable armor in seawater under weak magnetic fields

Pengfei Li[a], Yuebin Chen[a], Haowei Huang[a], Huijuan Zhang[a,*], Hongwei Xie[a], Hong-Guang Piao[a,b,**]

[a] Hubei Engineering Research Center of Weak Magnetic-Field Detection, China Three Gorges University, Yichang 443002, China
[b] Department of Physics, College of Science, Yanbian University, Yanji 133002, China

ARTICLE INFO

Keywords:
Submarine cables
Seawater corrosion
Electrochemical corrosion
Magnetic field effects

ABSTRACT

Submarine cables are the main transmission channel for offshore wind power technology. In the actual work of submarine cables, it is inevitable that an induced magnetic field will be generated in the submarine cable armor. The induced magnetic field generated will have a certain impact on the corrosion of the submarine cable armor, thus affecting the service life of the submarine cable. In this paper, the corrosion behavior of submarine cable armor with galvanized steel structure in seawater under different weak magnetic fields is investigated by electrochemical corrosion experiments. The results show that the galvanized layer does not play a protective role when the structure of submarine cable armor is damaged, and the magnetic field environment plays a role in promoting the corrosion behavior of submarine cable armor. Through the analysis of its corrosion mechanism, it is found that the magnetic field promotes the corrosion behavior of submarine cable armor by affecting charge transfer and the formation of corrosion products, which provides a reference for the accurate evaluation of the actual service life of submarine cable.

1. Introduction

With the rise of offshore wind power technology, submarine cables have developed rapidly. Submarine cable is the main channel for power transmission and signal transmission of offshore platforms [1,2]. However, due to severe corrosion of the submarine cable armor, the rupture of the submarine cable has caused frequent accidents in offshore power transmission and signal transmission paralysis in recent years [3–6], causing serious economic losses. The corrosion protection of submarine cable and the corrosion of the submarine cable armor in its working environment have attracted much attention in recent years [7–9]. As is known to all, the submarine cable is laid on the seabed, the complex environment of the sea, the high salinity of the sea water, the abundance of Cl^- [10] the frequent activity of marine microorganisms and other reasons will accelerate the corrosion of the submarine cable armor [11–13]. In addition, the induced magnetic field or electric field will inevitably be generated in the process of electrical transport of submarine cable, and their existence must play a role in the corrosion of submarine cable armor [14,15]. Many researchers have reported the corrosion process of submarine cables in various environments [15–18]. For example, Jiang et al. studied the corrosion of armor by induced current [15]; Zhu et al. studied the AC interference mode and safe distance of high-voltage AC cables in submarine pipelines [16]; Guo et al. conducted an electrochemical noise study on the complex galvanic corrosion of the armor layer of Submarine communications cable in artificial seawater [17]; Reda et al. conducted research on the design of in-service worn Submarine communications cable/umbilical [18]. As one of the most commonly used materials in submarine cables, the corrosion of galvanized steel has attracted much attention and many related reports have been made. For example, Sabzi, et al. have used potentiodynamic polarization and electrochemical impedance spectroscopy to study the effect of temperature on the corrosion behavior of galvanized steel in seawater environment [19]; Neupane, et al. have studied the effects of NH_4^+, Na^+, and Mg^{2+} ions on the corrosion behavior of galvanized steel in wet-dry cyclic conditions [20]; Kartsonakis, et al. have studied a comparative study of corrosion inhibitors on hot-dip galvanized steel [21] and so on. However, the effect of magnetic field on the corrosion behavior of galvanized steel is rarely studied and its mechanism is still unclear.

Since the magnetic field plays a certain role in the corrosion

* Corresponding author.
** Corresponding author at: Hubei Engineering Research Center of Weak Magnetic-Field Detection, China Three Gorges University, Yichang 443002, China.
E-mail addresses: zhanghuijuan82@126.com (H. Zhang), hgpiao@ybu.edu.cn (H.-G. Piao).

https://doi.org/10.1016/j.ijoes.2023.100264
Received 26 May 2023; Received in revised form 20 June 2023; Accepted 27 June 2023
Available online 29 June 2023

behavior of metals and has little impact on the natural environment, it has recently attracted the attention in the field of green anticorrosion technology research and development [22–26]. Recent research results have found that magnetic fields can promote the corrosion of metals in some cases, and can inhibit the corrosion of metals in other cases. The reason for the different corrosive effects of magnetic fields is caused by different corrosion conditions and environments. Such as the main causes of promoting corrosion include the application of a magnetic field enhances the dissolution of the surface film, which decreased the surface film coverage fraction and made the electrode prone to active dissolution [23], and accelerates the mass transport processes at the precipitation-dissolution type surface film/solution interfaces [24]. In other cases, the magnetic field can inhibit the corrosion of metals by affecting the adsorption process of the intermediate [25] and the electrical migration of the electrode surface [26]. This is an important technical problem that must be overcome for the development and application of magnetic field anticorrosion technology. Therefore, understanding and controlling the effect of magnetic field on the corrosion behavior of galvanized steel in seawater environment is one of the key considerations for the accurate assessment of the service life of submarine cables in electromagnetic environment.

In this work, we have systematically investigated the effect of magnetic field on the corrosion behavior of submarine cable armor with galvanized steel structure under seawater environment, and revealed its mechanism by microstructural characterization and electrochemical analysis. It will provide a technical reference for the accurate evaluation of the actual service life of submarine cable.

2. Experimental

2.1. Preparation of samples

The corrosion sample, galvanized steel wire of submarine cable armor (diameter 5.00 mm, Tianjin Huayuan Times Metal Products Co., Ltd, China), complies with the preparation standard of GB/T 3082–2020. Firstly, the galvanized steel wire was cut into a small cylindrical sample with a length of 10 mm by using the Wire Electrical Discharge Machining (WEDM). Then, the reaction surface (galvanized steel wire cross section) was polished to the mirror surface with sandpaper with different mesh numbers, from 400 mesh gradually increase to 3000 mesh, to eliminate the influence of rough surface on the electrochemical experimental measurement. Finally, all samples were washed with deionized water and ethanol to remove oil stains and other impurities. In this paper, the cross-section (round surface, diameter 5.0 mm) was selected as the reaction surface, and other surfaces were covered with epoxy resin (1:1 ratio of epoxy resin and polyamide resin). The corrosion solution is made of artificial sea water mixed with natural sea salt (Weifang Huanyu Salt Chemical Co., Ltd , China) and deionized water. The concentration of the artificial seawater at room temperature is 30 g/L, and the pH value is 8.2. We found that the NaCl concentration in the artificial seawater was ~2.4 % as measured by a high-precision salinity meter (Chizhou Jiuhua optical instrument Co. Ltd. JHGXT-2832YATC, China). Ultrasonic stirring was performed during the solution preparation and the solution was exposed to static air during the experiment. The magnetic field (B) is provided by two permanent magnets (NdFeB, B ≈ 98.9 mT at the sample position) or an electromagnet (East Changing Technologies EM-3, China) with the Keithley 2400 source meter as the power source. The direction of the external B application is parallel to the reaction surface (yellow part), as shown in Fig. 1.

2.2. Electrochemical experiments

The corrosion test and analysis of samples were performed by using the electrochemical Bipotentiostat (Shanghai Chenhua Instruments Ins. Model 760e, China) under different B conditions provided by the electromagnet. Here, three-electrode Teflon cell method has been adopted [27], such as the corrosion sample was used as the working electrode, the circular platinum electrode with a diameter of 10 mm as the counter electrode, and the saturated calomel electrode (SCE) as the reference electrode. The experiments of potentiostatic polarization curve, potentiodynamic polarization curve and electrochemical impedance spectroscopy (EIS) all wait (~1200 s) for the open circuit potential of the test sample to stabilize before starting the measurement. The measured initial voltage of the potentiostatic polarization curve and EIS are set as the voltage when the open-circuit potential is stable. The test time of the potentiostatic polarization curve is 500 s with dynamically turn on/off the B = 20, 40 and 60 mT (the B turn on at 200 s and off at 350 s). The initial voltage of potentiodynamic polarization curve is −1.5 V (*vs* SCE), the ending voltage is −0.5 V (*vs* SCE), and the scanning rate is 0.01 V • s^{-1}. The measurement range of EIS is 10^{-1} ~10^{5} Hz, the amplitude is 5 mV, and the scanning rate is 1 mV•s^{-1}. All the above experiments were repeated many times to reduce the experimental error and ensure the reliability of the experiments.

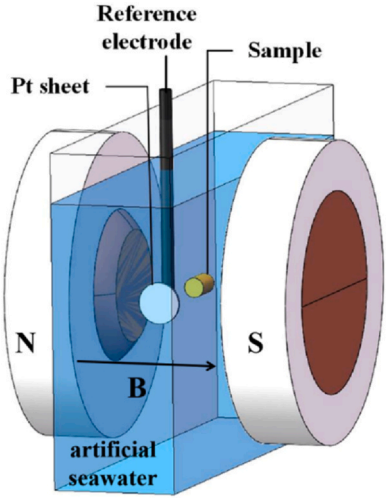

Fig. 1. Schematic diagram of electrochemical tests based on three-electrode Teflon cell method under different B conditions.

2.3. Morphology and microstructure characterization

After the samples were soaked in artificial seawater for 24 h under B = 0 mT or B ≈ 98.9 mT conditions provided by two NdFeB magnets, the corrosion morphology of its surface is observed by using the scanning electron microscope (SEM, JEOL JSM-7500 F, Japan). The chemical composition of the sample surfaces before or after corrosion is characterized and compared by the energy dispersive X-Ray spectroscopy (EDS, Oxford Instruments) equipped in the SEM and the X-ray powder diffraction (XRD, Rigaku Ultima IV, Japan) with a conventional Cu-Kα radiation source.

3. Results and discussion

3.1. Electrochemical polarization measurements

Fig. 2(a) and (b) give the potentiostatic polarization and potentiodynamic polarization curves measured under different B strengths, respectively. In quasi-steady state measurements of potentiostatic polarization, the initial potential was set to U_0 = −1.03 V (*vs* SCE). The B is applied at 200 s and removed at 350 s. As shown in Fig. 2(a), it can be observed that the B = 20 mT has almost no effect on the corrosion current density (***j***), which is different from cases of B = 40 mT and 60 mT. It is obvious that the ***j*** is negatively shifted with the enhancement

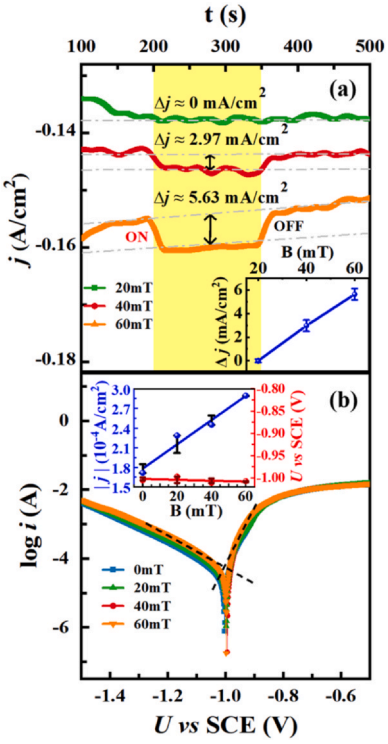

Fig. 2. (a) Shows potentiostatic polarization curves with dynamically turn on/off the B = 20, 40 and 60 mT under −1.03 V. The inset of (a) shows Δ***j*** value changes with the B. (b) Shows the potentiodynamic polarization curves under B = 0, 20, 40 and 60 mT. The inset of (b) shows the variation trend of corrosion current density |***j***| and corrosion potential (*U*) with the B.

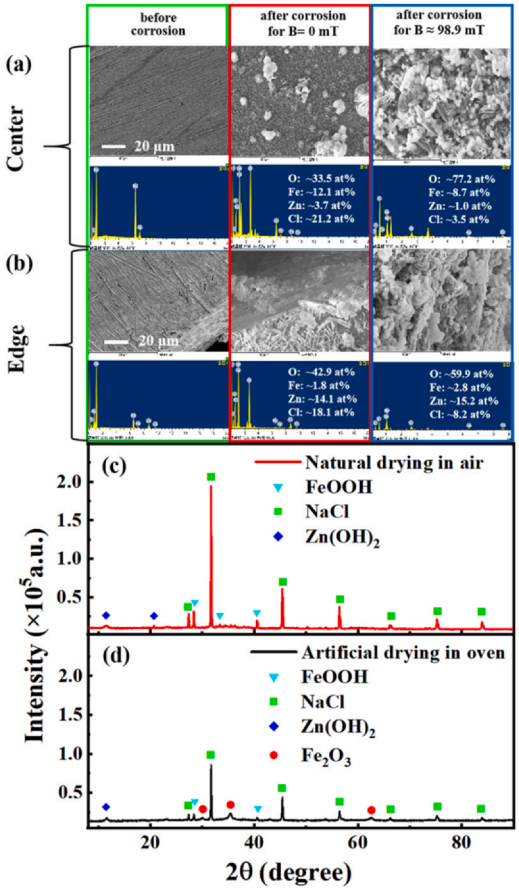

Fig. 3. Morphologies and main elemental compositions (for O, Fe, Zn, Cl elements) of corrosion products on the corrosion surface at the center and edge parts of the submarine cable armor under B = 0 mT and B ≈ 98.9 mT. (c) and (d) show the chemical composition of corrosion products for the natural air drying at room temperature and the artificial oven drying at 70 °C, respectively.

of the B, but recovers when the B is removed. The ***j*** change value (Δ***j***) is about 2.97 and 5.63 mA/cm^2 for B = 40 mT and B = 60 mT cases, respectively. It is found that the Δ***j*** presents a linear increasing trend on the B strength, as shown in the inset of Fig. 2(a). This indicates that the corrosion rate of galvanized steel increases with the increase of B strength, which means that the B can promote the corrosion of submarine cable armor in seawater environment.

The potentiodynamic polarization curve can more intuitively show the effect of different B on the corrosion behavior of galvanized steel, as shown in Fig. 2(b). By the Tafel linear extrapolation, the absolute value of corrosion current density |***j***| and corrosion potential *U* (*vs* SCE) can be obtained under different B strengths, as shown the inset of Fig. 2(b). It is obvious that there is a linear dependence between the |***j***| and B strength (see the blue line), whereas the *U* has almost no response to the B (see the red line). This means that the B mainly affects the ***j*** of the submarine cable armor rather than the *U* during electrochemical corrosion. It is consistent with the conclusion of potentiostatic polarization experiment, and further verifies that B can promote the corrosion of submarine cable armor in seawater environment.

3.2. Characterizations of morphology and microstructure

In order to further verify the effect of B on corrosion of submarine cable armor, the corrosion surface morphology and the element composition of corrosion products were characterized by SEM and EDS at the center and edge parts of submarine cable armor samples after soaking 24 h in artificial seawater. It can be seen from the SEM morphologies that the center and edge surfaces of the sample before corrosion are smooth and flat, as shown in the green box of Fig. 3(a) and (b). However, the morphology of the corrosion products on the sample surface after corrosion becomes rougher than that before corrosion, and its structure also becomes loose, as shown in the red and blue boxes of Fig. 3(a) and (b), respectively. It can be seen from the comparison of morphologies in Fig. 3(a) and (b) that the corrosion at the edge of the sample is more serious than that at the center. Through the comparison of SEM morphologies, it can be observed that some corrosion products appear on the sample surface under the no-B condition, while a large number of corrosion products even form petal-like structures [22] under the B condition. EDS composition analysis shows that the surface corrosion products are mainly composed of Fe, Zn, O and Cl elements. In addition, it is found that the percentage content of Fe and Zn atoms in the center of the sample corrosion surface is significantly different from at the sample edge. From the EDS data in Fig. 3(a) for center and 3(b) for edge, it can be observed that the center of the submarine cable armor is dominated by Fe, and the edge is dominated by Zn, which is in line with the structural characteristics of the submarine cable armor itself. The presence of a large number of Cl elements can be attributed to the precipitation of NaCl from the simulated seawater on the sample surface after the corrosion experiment [22]. What is most notable here is the difference in O content on different parts of the sample corrosion surface. It can be observed that the contents of O atoms at the center and edge parts are 33.5 at % and 42.9 at % (77.2 at % and 59.9 at %) without the B (with the B), respectively. It is obvious that the overall O content in the B presence is greater than that in the B absence, which means that the B promotes the corrosion of submarine cable armor. In addition, it is found that the O content at the center of the corrosion surface is greater than that at the edge of the sample, that is, the corrosion rate at the center is greater than that at the edge, which can be attributed to the non-uniform distribution of the B around the galvanized steel caused by its internal magnetization [28].

To confirm the composition of corrosion surface products, we analyzed the corrosion products using XRD and divided them into two treatment methods: the natural air drying at room temperature and the artificial oven drying at 70 ˚C, as shown in Fig. 3(c) and (d). In the case of natural drying in air (see Fig. 3(c)), the products on the sample surface are mainly composed of NaCl, FeOOH, and $Zn(OH)_2$. In the case of artificial oven drying (see Fig. 3(d)), it is mainly composed of NaCl, FeOOH, $Zn(OH)_2$ and Fe_2O_3. Here, the NaCl comes from seawater, the FeOOH is an intermediate product, the $Zn(OH)_2$ is corrosion product of Zn, and the Fe_2O_3 is the product generated by further oxidation of FeOOH. The reaction process is as follows [28,29]:

$$Fe \rightarrow Fe^{2+} + 2e^{-}; \quad (1)$$

$$Fe^{2+} \rightarrow Fe^{3+} + e^{-}; \quad (2)$$

$$Fe^{3+} + 3(OH)^{-} \rightarrow FeOOH + H_2O; \quad (3)$$

$$Fe^{2+} + 8FeOOH + 2e^{-} \rightarrow 3Fe_3O_4 + 4H_2O; \quad (4)$$

$$4Fe_3O_4 + O_2 \rightarrow 6Fe_2O_3; \quad (5)$$

$$Zn \rightarrow Zn^{2+} + 2e^{-}; \quad (6)$$

$$O_2 + 2H_2O + 4e^{-} \rightarrow 4(OH)^{-}; \quad (7)$$

$$Zn^{2+} + 2(OH)^{-} \rightarrow Zn(OH)_2. \quad (8)$$

Therefore, it can be considered that the B influences the corrosion behavior of carbon steel substrate mainly by modulating the formation and densification of corrosion intermediates (FeOOH).

3.3. Electrochemical impedance spectroscopy

In order to clarify the corrosion process and mechanism of the magnetic field on the submarine cable armor in the seawater environment, the EIS was measured under the magnetic field of B = 0 mT, 20 mT, 40 mT, and 60 mT, as shown in Fig. 4.

Based on the above observation data and analysis results, an equivalent circuit model is established, as shown in the inset of Fig. 4(a). It can be observed from the Nyquist plots (see Fig. 4(a)) that two capacitive arcs can appear in the high- and low-frequency regions under different B strengths. The capacitive arc in the high-frequency region is generally caused by charge transfer in the double layer capacitance of the electrode [30]. Due to the structural characteristics of galvanized steel for submarine cable armor, in our case, there should be two capacitive arcs located in the high-frequency region of the EIS, as shown in phase angle Bode plots of the Fig. 4(b). This means that the capacitive arc at the highest frequency region is coming from a double layer on the surface of the galvanized layer and the other one comes from the carbon steel core. In addition, another capacitive arc was observed was observed in the low-frequency region of the EIS, as shown in Fig. 4(a) and (b). The capacitive arc located in the low-frequency region are generally attributed to the corrosion product layer adsorbed on the reaction surface due to delayed diffusion [31], such as FeOOH and $Zn(OH)_2$ in our case. The profiles of EIS curves are similar under different B strengths, indicating that the corrosion mechanism does not change with the B change. From the Bode plots, it is found that the impedance |Z| at 0.1 Hz decreases gradually with increasing the B strength, which indicate that the corrosion rate of the submarine cable armor is promoted by the magnetic field [32].

The EIS data at different B strengths have been fitted according to the equivalent circuit, the fitting parameters are presented in Table 1. In the equivalent circuit model, R_s is the solution resistance; R_{ct1} and CPE_{dl1} correspond to charge transfer resistance and double layer capacitance of Zn corrosion in the Zn-Fe galvanic corrosion; R_{ct2} and CPE_{dl2} correspond to the charge transfer resistance and double layer capacitance of the corrosion process of carbon steel substrate; R_m and CPE_m correspond to the resistance and capacitance of the corrosion

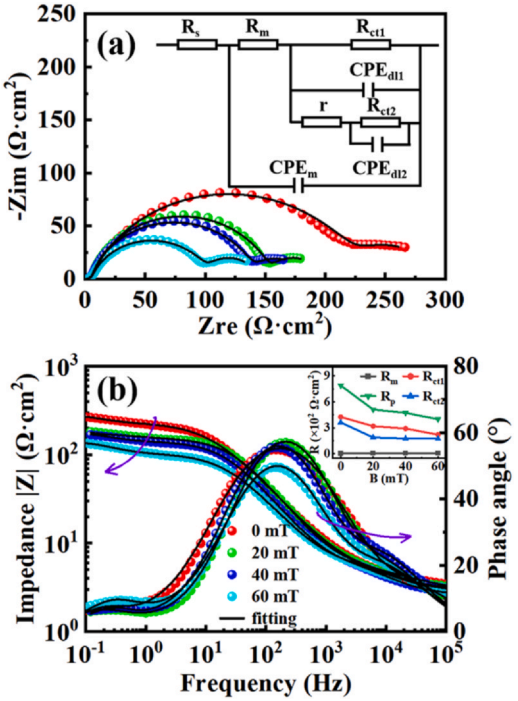

Fig. 4. (a) Nyquist plots and (b) Bode plots under B = 0, 20, 40 and 60 mT. The top inset of (a) shows the equivalent circuit model. The top inset of (b) shows the resistance changes under B = 0, 20, 40 and 60 mT. The black lines are fitting curves.

product film during the reaction. Here, the constant phase element (CPE) is instead of the capacitor element because the electrode surface is rough and uneven [33]. Because of the difference in the chemical activity of Zn and Fe, the r can represent the difference in their chemical reaction with the corrosion solution. Generally, R_{ct} is used to evaluate the corrosion performance, while R_m reflects the deposition degree of corrosion products on the surface of the working electrode. Therefore, $R_p = R_{ct1} + R_{ct2} + R_m$ is used to evaluate the corrosion performance of the submarine cable armor in this paper [34]. From the Table 1, it can be seen that the value of R_p decreases gradually with increase of the B strength, indicating that the B promotes the corrosion of submarine cable armor, which is completely consistent with the above two experimental conclusions. In addition, it was found that the R_m value was not only small but also did not change much with the B change, indicating that no dense corrosion products were formed on the sample surface. Interestingly, the resistance values of R_{ct1} and R_{ct2} are significantly decreased with the increase of the B strength, as shown in the inset of Fig. 4(b). Under ΔB = 60 mT change, R_{ct1} decreased from 425 Ω·cm² to 220 Ω·cm², which is reduced by about 1.93 times; R_{ct2} decreased from 361.2 Ω·cm² to 173.2 Ω·cm², which is reduced by about 2.09 times. According to the above results, it can be determined that the B can accelerate the corrosion rate of submarine cable armor by promoting the charge transfer of the double electric layer and inhibiting the formation of the dense corrosion product layer on the surface of galvanized steel. The conclusions are completely consistent with the results of electrochemical testing and composition analysis of the corrosion products.

3.4. Mechanism analysis

Based on the above results, the corrosion mechanism of galvanized steel is analyzed after the protective effect of galvanized layer fails, as shown in Fig. 5. The top gray area in the cross-sectional schematic diagram of the submarine cable armor represents the epoxy resin coating layer. The middle blue area represents the galvanized layer, and

Table 1
Analysis data of EIS with different magnetic field.

B	R_s	R_m	CPE_m		R_{ct1}	CPE_{dl1}		r	R_{ct2}	CPE_{dl2}		R_p
(mT)	(Ω·cm^2)	(Ω·cm^2)	Y_m ($S^n\Omega^{-1}$cm^{-2})	n_m	(Ω·cm^2)	Y_{dl1} ($S^n\Omega^{-1}$cm^{-2})	n_{dl1}	(Ω·cm^2)	(Ω·cm^2)	Y_{dl2} ($S^n\Omega^{-1}$cm^{-2})	n_{dl2}	(Ω·cm^2)
0	2.96	2.7	3.6×10^{-5}	0.78	425	1.2×10^{-4}	0.77	491	361.2	4.2×10^{-3}	0.90	788.9
20	3.02	4.6	3.7×10^{-5}	0.82	318.2	5.2×10^{-5}	0.86	279	187.6	7.0×10^{-3}	0.91	510.4
40	2.58	5.6	6.2×10^{-5}	0.78	290.8	6.4×10^{-5}	0.87	253.8	175.7	7.0×10^{-3}	0.91	472.1
60	2.84	5.3	1.0×10^{-4}	0.74	220	1.0×10^{-4}	0.83	174	173.2	2.5×10^{-3}	0.93	398.5

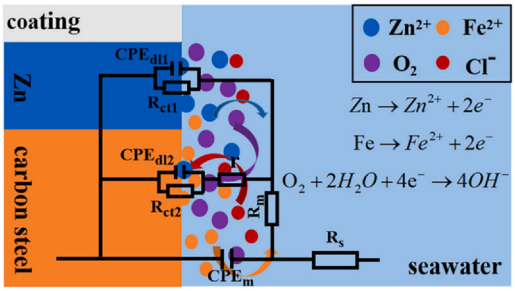

Fig. 5. Corrosion mechanism diagram of the exposed galvanized steel substrate.

the bottom orange area represents carbon steel core. In the figure, the blue arrow shows the direction of Zn^{2+} movement during the reaction [35]. The red arrow shows the direction of Cl^- movement. The content of Zn in the submarine cable armor is much less than that in carbon steel, and the galvanized layer cannot play a cathodic protection role on carbon steel core [36], so the carbon steel core will be corroded under the constant attack of Cl^- in seawater [37]. The orange arrow and the purple arrow express the moving direction of Fe^{2+} and O_2 during the reaction, respectively. The movement of Fe^{2+} causes it to further oxidize to Fe^{3+}, which eventually adsorbs on the center of the reaction surface as FeOOH. Here, the $Zn(OH)_2$ corrosion products in the galvanized layer are mainly adsorbed to the edge of the corrosion surface. The comparison between the center (see Fig. 3(a)) and the edge (see Fig. 3(b)) morphologies of corrosion surface shows that the corrosion products at the edge are more and denser than those at the center, which means that galvanized layer locally plays a cathodic protection role.

4. Conclusions

In this paper, the effect of different B strengths on the corrosion characteristics of submarine cable armor in seawater environment has been investigated by electrochemical experiments and microstructure characterization. The results show that the B promotes the charge transfer during the galvanized steel reaction and inhibits the formation of the dense corrosion product on the surface. In practice, the submarine cable will inevitably generate induced magnetic field around it. Therefore, the exploration of the influence of B on the corrosion behavior of galvanized steel in seawater environment will provide an important reference for accurately evaluating the service life of submarine cables in electromagnetic environment.

Declaration of Competing Interest

The authors declare that they have no known competing financial interests or personal relationships that could have appeared to influence the work reported in this paper.

Acknowledgments

This work was supported by the National Key R&D Program of China (Grant No. 2017YFB0903700 and 2017YFB0903702) and the Research Project at Yanbian University of China (Grant No. 482022104). P.F.L. and Y.B.C. contributed equally to this paper.

References

[1] W. Wang, X. Yan, S. Li, L. Zhang, J. Yang, X. Ni, Failure of submarine cables used in high-voltage power transmission: characteristics, mechanisms, key issues and prospects, IET Gener. Transm. Distrib. 15 (2021) 1387–1402, https://doi.org/10.1049/gtd2.12117

[2] D.R. Burnett, R.C. Beckman, T. Davenport, Submarine cables: the handbook of law and policy, Leiden. Martinus Nijhoff Publ. (2014), https://doi.org/10.1163/9789004260337?nosfx=y

[3] B. Gustavsen, M. Høyer-Hansen, M. Hatlo, S. Midttveit, Voltages and AC corrosion on metallic tubes in umbilical cables caused by magnetic induction from power cable charging currents, IEEE Trans. Power Deliv. 34 (2018) 596–605, https://doi.org/10.1109/TPWRD.2018.2881221
[4] Y. Liao, S. Bao, Y. Xie, Y. Zhao, P. Wang, G. Liu, B. Hui, Y. Xu, Breakdown failure analysis of 220 kv cable joint with large expanding rate under closing overvoltage, Eng. Fail. Anal. 120 (2021) 105086, https://doi.org/10.1016/j.engfailanal.2020.105086
[5] Y. Chen, B. Hui, Y. Cheng, Y. Hao, M. Fu, L. Yang, S. Hou, L. Li, Failure investigation of buffer layers in high-voltage XLPE cables, Eng. Fail. Anal. 113 (2020) 104546, https://doi.org/10.1016/j.engfailanal.2020.104546
[6] E.L. Pope, P.J. Talling, L. Carter, Which earthquakes trigger damaging submarine mass movements: Insights from a global record of submarine cable breaks? Mar. Geol. 384 (2017) 131–146, https://doi.org/10.1016/j.margeo.2016.01.009
[7] H.S. Yoon, W.-B. Na, Safety assessment of submarine power cable protectors by anchor dragging field tests, Ocean Eng. 65 (2013) 1–9, https://doi.org/10.1016/j.oceaneng.2013.03.004
[8] E.C. Bascom, R.J. Schwabe, J.F. Troisi, A.V. Poliakov, S. Zelingher, S.A. Dave, Submarine cable cathodic protection, IEEE Comput. Appl. Power 14 (2001) 39–43, https://doi.org/10.1109/67.893354
[9] H.S. Yoon, W.B. Na, Anchor drop tests for a submarine power-cable protector, Mar. Technol. Soc. J. 47 (2013) 72–80, https://doi.org/10.4031/MTSJ.47.3.6
[10] D.H. Xia, Z. Qin, S. Song, D. Macdonald, J.L. Luo, Combating marine corrosion on engineered oxide surface by repelling, blocking and capturing Cl^-: a mini review, Corros. Comm. 2 (2021) 1–7, https://doi.org/10.1016/j.corcom.2021.09.001
[11] Q. Zhang, X. Wang, W. Du, H. Zhang, X. Li, Reliability Model of Submarine Cable Based on Time-varying Failure Rate, 2019 IEEE 8th International Conference on Advanced Power System Automation and Protection (APAP). IEEE, (2019) 711–715. https://doi.org/10.1109/APAP47170.2019.9224914.
[12] E.C. Bascom, Y. Iossel, A.V. Poliakov, J.F. Troisi, R.J. Schwabe, Construction features and environmental factors influencing corrosion on a self-contained fluid, IEEE Trans. Power Deliv. 13 (1998) 677–682, https://doi.org/10.1109/61.686959
[13] Z. Zhang, N. Li, L. Liu, T. Li, Y. Cong, Modal and harmonic response analysis of submarine cable under multiple working conditions, In 2022 IEEE Sustainable Power and Energy Conference (iSPEC). IEEE, (2022) 1–6. https://doi.org/10.1109/iSPEC54162.2022.10032982.
[14] Y. Chen, K. Zhou, J. Kong, S. Akram, X. Ren, X. Zhang, Y. Li, Q. Zhao, Hydrogen evolution and electromigration in the corrosion of aluminium metal sheath inside high-voltage cables, High. Volt. 7 (2022) 260–268, https://doi.org/10.1049/hve2.12163
[15] Z. Jiang, S. Dong, Y. Zhang, G. Liu, T. Dong, Corrosion of copper armor caused by induced current in a 500 kv alternating current submarine cable, Electr. Power Syst. Res. 195 (2021) 107144https://doi.org/107144.10.1016/j.epsr.2021.107144.
[16] Z. Zhu, Y. Liang, L. Chen, Y. Liu, Y. Du, Study on AC interference law of high voltage AC cable to submarine pipeline and safe distance, Mater. Corros. 74 (2023) 560–575, https://doi.org/10.1002/maco.202213559
[17] R. Guo, P. Yang, F. Mao, J. Li, L. Chen, G. Yun, D. Macdonald, Electrochemical noise studies on complex galvanic corrosion of submarine cable armor layer in artificial seawater, Mater. Corros. 73 (2022) 379–392, https://doi.org/10.1002/maco.202112803
[18] A. Reda, M.A. Elgazzar, J. Thiedeman, K.K. McKee, I.A. Sultan, M.A. Shahin, Design of subsea cables/umbilicals for in-service abrasion-Part 2: mechanisms, Ocean Eng. 234 (2021) 109098, https://doi.org/10.1016/j.oceaneng.2021.109098
[19] M. Sabzi, S.M. Dezfuli, M. Asadian, A. Tafi, A. Mahaab, Study of the effect of temperature on corrosion behavior of galvanized steel in seawater environment by using potentiodynamic polarization and EIS methods, Mater. Res. Express 6 (2019) 076508, https://doi.org/10.1088/2053-1591/ab10ad
[20] S. Neupane, S. Hastuty, N. Yadav, N. Singh, A.P. Yadav, Effects of NH_4^+, Na^+, and Mg^{2+} ions on the corrosion behavior of galvanized steel in wet-dry cyclic conditions, Mater. Corros. 72 (2021) 1388–1395, https://doi.org/10.1002/maco.202112360
[21] I.A. Kartsonakis, S.G. Stanciu, A.A. Matei, R. Hristu, A. Karantonis, C.A. Charitidis, A comparative study of corrosion inhibitors on hot-dip galvanized steel, Corros. Sci. 112 (2016) 289–307, https://doi.org/10.1016/j.corsci.2016.07.030
[22] S. Zhao, Y. Wang, Y. Zhao, X. Sun, H. Zhang, H.-G. Piao, Y. Zhang, Y. Huang, The effect of magnetic field pretreatment on the corrosion behavior of carbon steel in static seawater, RSC Adv. 10 (2020) 2060–2066, https://doi.org/10.1039/C9RA09079G
[23] Z. Lu, D. Huang, Y. Wu, J. Congleton, Effects of an applied magnetic field on the dissolution and passivation of iron in sulphuric acid, Corros. Sci. 45 (2003) 2233–2249, https://doi.org/10.1016/S0010-938X(03)00045-3
[24] Z. Lu, C. Huang, D. Huang, Y. Wu, Effects of a magnetic field on the anodic dissolution, passivation and transpassivation behaviour of iron in weakly alkaline solutions with or without halides, Corros. Sci. 48 (2006) 3049–3077, https://doi.org/10.1016/j.corsci.2005.11.014
[25] R. Sueptitz, K. Tschulik, M. Uhlemann, J. Eckert, A. Gebert, Retarding the corrosion of iron by inhomogeneous magnetic fields, Mater. Corros. 65 (2014) 803–808, https://doi.org/10.1002/maco.201206890
[26] R. Sueptitz, K. Tschulik, M. Uhlemann, L. Schultz, A. Gebert, Magnetic field effects on the active dissolution of iron, Electrochim. Acta 56 (2011) 5866–5871, https://doi.org/10.1016/j.electacta.2011.04.126
[27] X. Zhang, Z. Wang, Z. Zhou, G. Yang, X. Cai, Impact of magnetic field on corrosion performance of Al-Mg alloy with different electrode potential phases, Intermetallics 129 (2021) 107037, https://doi.org/10.1016/j.intermet.2020.107037
[28] H.W. Huang, H. Zhang, P. Li, Y. Chen, S. Zhao, X. Sun, H.-G. Piao, X. Zhao, Y. Huang, Effects of lorentz force and gradient force of magnetic field on seawater corrosion behavior of carbon steels, Corrosion (2023) 4285, https://doi.org/10.5006/4285
[29] Y. Meng, L. Liu, D. Zhang, C. Dong, Y. Yan, A.A. Volinsky, L.-N. Wang, Initial formation of corrosion products on pure zinc in saline solution, Bioact. Mater. 4 (2019) 87–96, https://doi.org/10.1016/j.bioactmat.2018.08.003
[30] Y. Xin, T. Hu, P.K. Chu, Degradation behaviour of pure magnesium in simulated body fluids with different concentrations of $HCO3^-$, Corros. Sci. 53 (2011) 1522–1528, https://doi.org/10.1016/j.corsci.2011.01.015
[31] G. Baril, N. Pébère, The corrosion of pure magnesium in aerated and deaerated sodium sulphate solutions, Corros. Sci. 43 (2001) 471–484, https://doi.org/10.1016/S0010-938X(00)00095-0
[32] S. Wang, Y. Gu, Y. Geng, J. Liang, J. Zhao, J. Kang, Investigating local corrosion behavior and mechanism of MAO coated 7075 aluminum alloy, J. Alloy. Compd. 826 (2020) 153976, https://doi.org/10.1016/j.jallcom.2020.153976
[33] X. Yu, Z. Wang, Z. Lu, Atmospheric corrosion behavior of copper under static magnetic field environment, Mater. Lett. 266 (2020) 127472, https://doi.org/10.1016/j.matlet.2020.127472
[34] J. Li, F. Xie, D. Wang, C. Ma, M. Wu, K. Gong, Effect of magnetic field on stress corrosion cracking induced by sulfate-reducing bacteria, Constr. Build. Mater. 303 (2021) 124521, https://doi.org/10.1016/j.conbuildmat.2021.124521
[35] N.C. Barnard, S.G.R. Brown, Modelling the relationship between microstructure of galfan-type coated steel and cut-edge corrosion resistance incorporating diffusion of multiple species, Corros. Sci. 50 (2008) 2846–2857, https://doi.org/10.1016/j.corsci.2008.07.005
[36] A.P. Yadav, A. Nishikata, T. Tsuru, Electrochemical impedance study on galvanized steel corrosion under cyclic wet-dry conditions–influence of time of wetness, Corros. Sci. 46 (2004) 169–181, https://doi.org/10.1016/S0010-938X(03)00130-6
[37] A.P. Yadav, A. Nishikata, T. Tsuru, Degradation mechanism of galvanized steel in wet-dry cyclic environment containing chloride ions, Corros. Sci. 46 (2004) 361–376, https://doi.org/10.1016/S0010-938X(03)00153-7